Journal of ELECTRONIC MATERIALS, Vol. 48, No. 5, 2019
https://doi.org/10.1007/s11664-019-07115-8

TOPICAL COLLECTION: 60TH ELECTRONIC MATERIALS CONFERENCE 2018

Deposition of β-Polyfluorene by Resonant Infrared Matrix-Assisted Pulsed Laser Evaporation

SPENCER FERGUSON,[1] CASSANDRA V. WILLIAMS,[1] BATAUNG MOHAPI,[2] and ADRIENNE D. STIFF-ROBERTS [1,3,4]

1.—Department of Electrical and Computer Engineering, Duke University, Durham, NC 27708, USA. 2.—Department of Mechanical Engineering and Materials Science, Duke University, Durham, NC 27708, USA. 3.—University Program in Materials Science and Engineering, Duke University, Durham, NC 27708, USA. 4.—e-mail: adrienne.stiffroberts@duke.edu

Emulsion-based, resonant infrared matrix-assisted pulsed laser evaporation (RIR-MAPLE) was used to deposit thin films of polyfluorene (PFO) with semi-crystalline phase domains (β-PFO), which has been performed, previously, only by solution phase processing. Various target emulsion recipes were studied, with emphasis on the primary solvent choice, emulsion mixing time, secondary solvent concentration, or total water concentration. The emulsified particle size for each recipe was compared using dynamic light scattering. Additionally, elevated growth temperature of the substrate was considered for controlling film formation. The surface quality of films was determined by atomic force microscopy, and β-PFO concentration was monitored using photoluminescence or UV–visible absorbance spectroscopy. Importantly, in contrast to solution-based deposition of β-PFO in thin films, emulsion-based RIR-MAPLE demonstrated the ability to increase β-PFO content without degrading, simultaneously, the surface properties of the films. This initial result helps establish the ability of RIR-MAPLE to control and promote semi-crystalline phases in polymer films.

Key words: RIR-MAPLE, matrix-assisted pulsed laser evaporation, PFO, polyfluorene, emulsions, semi-crystalline phases

INTRODUCTION

Semi-crystalline behavior in conjugated polymers has been an important topic of research for many years. Polymers such as poly(vinylidene fluoride) (PVDF)[1–4] and polyfluorene (PFO)[5,6] have been studied for their semi-crystalline features, which enhance certain properties of the polymers. PFO is considered a strong candidate for blue polymer light emitting diodes (LEDs) due to its high color purity and photoluminescence quantum yield.[7] Amorphous PFO (α-PFO) is the standard phase of the polymer that lacks order. The semi-crystalline phase, denoted β-PFO, forms by the planarization of molecular chains in solution, provided that the solvent allows self-interactions to occur.[8] The semi-crystalline β-PFO phase is desirable because, even in small concentrations, β-PFO dominates the optical characteristics of thin films due to significantly higher carrier mobilities throughout the planarized phase domains.[9] Additionally, due to a shift in the conjugation length of β-PFO during planarization of the PFO backbone, the band gap of the polymer red shifts, allowing optical characterization, such as UV–Vis absorbance and photoluminescence spectroscopies, to be used to determine the presence of β-PFO.[8,10–12] In limited device studies, this change in carrier transport has resulted in increased color purity, brightness (34,326 cd m^{-2}), luminous efficiency, and external quantum efficiency (3.33%) in LEDs.[11,13] In addition, improved carrier transport should allow lower operating voltages,[11] thereby increasing device lifetime through decreased ohmic heating.[14,15]

(Received September 29, 2018; accepted March 6, 2019; published online March 14, 2019)

It has been shown that poor solvents of PFO, when evaporated slowly, allow sidechain interactions to occur, thus forming thin films with β-PFO phase domains.[8] Thus, β-PFO can be deposited via spin coating, drop casting or solvent annealing;[16] yet, all of these techniques degrade the film morphology[17] and limit the performance of devices due to increased contact resistance and scattering. A dipping process also has been used to attain semi-crystalline phases in spin-coated films, but the technique has not yielded β-PFO concentrations greater than 1.32%.[13] Alternatively, the synthesis of β-PFO can be induced by deposition with additives, such as quantum dots[18] or paraffin.[19] As a consequence of solution-based deposition via poor solvents, additives, or additional processing steps (such as solvent annealing), the morphology of thin films with β-PFO tend to have higher surface roughness than amorphous films, especially as the content of β-PFO increases. Moreover, if the concentration of β-PFO is too low (< 42% determined by UV–Vis absorbance measurements), the semi-crystalline phase within the thin film is not stable over time.[20]

Thus, while the incorporation of β-PFO at concentrations of approximately 42% (as determined by UV–Vis absorbance measurements) yields stabilization of the phase within thin films, thereby potentially improving the device performance of blue LEDs, higher film content of the semi-crystalline phase also yields degradation of surface characteristics due to the formation of pinholes.[20] Therefore, the ability to deposit thin-films with high content of β-PFO and high-quality surface morphology, simultaneously, is a significant challenge to taking advantage of these semi-crystalline phase domains within the context of blue LEDs.

Emulsion-based, resonant infrared matrix-assisted pulsed laser evaporation (RIR-MAPLE) is a potential solution for this challenge to the thin film deposition of β-PFO because it enables polymer/solvent combinations that are difficult to implement in more conventional, solution-based techniques. Emulsion-based RIR-MAPLE has been demonstrated as an alternative polymer deposition technique, and it allows for deposition of layered and bulk heterojunction structures without concern for compatibility of solvents.[21,22] In most MAPLE approaches, an ultraviolet (UV) laser is used to provide energy for evaporating a target matrix, i.e. a solvent in which the target organic material is dissolved. However, in many cases, the UV laser still provides enough energy for polymer chain scission. Instead, emulsion-based RIR-MAPLE uses an infrared laser to evaporate the continuous water–ice phase of a frozen emulsion comprising emulsified particles of a polymer that are transferred to the substrate. This gentle process has been shown to preserve the molecular weight[23] and chemical composition[24] of deposited polymers, and in the case of PFO, it prevents the oxidation during deposition that has been observed when UV lasers are used for the MAPLE deposition of α-PFO.[25,26] As an example, UV-MAPLE has been used to deposit PFO with various solvents, and β-PFO was observed in one film using tetrahydrofuan (THF) as the solvent matrix; however, oxidation of the PFO was also observed,[25,26] that is, PFO side chains reacted with oxygen causing the formation of a ketone group that led to the emission of green light from PFO.[27,28] Emulsion-based, RIR-MAPLE protects PFO, which is very sensitive to high energy processing due to this easy formation of a ketone group. Through the use of a low-energy, 2.94 μm infrared laser, the polymer does not interact with the laser energy directed at the target. Instead, the laser energy is resonantly absorbed by the hydroxyl bond vibrational modes present in the water–ice matrix of the target. The evaporation of the matrix then transfers emulsified polymer particles within the target such that they are gently deposited on a substrate.[24] With this emulsion-based approach, the polymer can be dissolved in a solvent ideal for the desired material properties. In order to emulsify these solutions, a surfactant is required to create a complex solution between polymer, nonpolar solvent, and water. While poor solvents are required to deposit β-PFO, emulsion-based RIR-MAPLE offers a unique opportunity to deposit PFO films without negatively affecting film morphology as the semi-crystalline phase is increased.

Previous work with RIR-MAPLE has shown a correlation between the simulated morphology of emulsions used as growth targets and film quality.[21] Specifically, dissipative particle dynamics (DPD) was used to simulate the effect of primary solvent solubility-in-water on emulsion droplet size. It was found experimentally that lower solubility-in-water correlated to smoother, denser films, and the simulation revealed that these emulsions comprised compact, spherical droplets. Such droplets are conducive to measuring particle size through dynamic light scattering (DLS).[21] Therefore, studying the effect of emulsion parameters on particle size and resulting film morphology for β-PFO will help in understanding the process-structure–property relationship of RIR-MAPLE for the controlled deposition of semi-crystalline polymer phase domains. The overall goal of this work is to identify emulsion conditions that yield pinhole-free, relatively smooth films in which the general surface morphology does not change significantly as the β-PFO content is increased.

EXPERIMENTAL METHODS

Materials

Poly(9,9-di-*n*-octylfluorenyl-2,7-diyl) (Product #571 652) Mw > 20,000, toluene, pseudocumene, cyclopentanone, o-dicholorobenzne,1,2,4 trichlorobenzene, phenol, and sodium dodecyl sulfate (SDS) were purchased

Table I. Primary solvent properties for PFO deposition by emulsion-based, RIR-MAPLE and resulting film surface morphology as measured by AFM (the indicated error represents the standard deviation for each measurement determined from three AFM images in different locations across the film)

Primary solvent	Vapor pressure (kPa)	Solubility-in-water (g/100 g)	Film thickness (nm)	Film roughness (nm)	Quality factor
Trichlorobenzene	0.038	0.00488	40.3 ± 0.4	15.2 ± 3.7	0.38
Pseudocumene	0.88	0.0057	261.7 ± 11.8	177.7 ± 25.3	0.68
Cyclopentanone	1.5	0.9175	151.7 ± 10.6	422 ± 154.6	2.78
Toluene	2.9	0.053	197.3 ± 32.3	250.4 ± 32.3	1.27
Dichlorobenzene	0.16	0.0156	21.5 ± 3.3	37.6 ± 8.5	1.75

from MilliporeSigma (Sigma-Aldrich). All materials were used as received.

Emulsion-Based RIR-MAPLE Target Recipe and Substrate Growth Temperature

The emulsion targets were prepared as follows: PFO was dissolved in a given solvent at the selected polymer:primary solvent concentration at 60°C and stirred at 400 RPM for 3 h in a nitrogen atmosphere to prevent oxidation. Phenol, the secondary solvent, was simultaneously heated until it liquified, at which point it was added to the polymer/primary solvent mixture at a ratio of 4:1 (primary solvent:secondary solvent) by %vol. The secondary solvent provides additional hydroxyl bonds to help resonantly absorb the laser energy, and its low vapor pressure helps prevent sublimation of the target. The secondary solvent concentration within the target emulsion was investigated also. The mixture was allowed to stir for different amounts of time while on a hotplate set to 35°C. A solution of sodium dodecyl sulfate (SDS) in water at 0.001% by weight was added to this mixture at a ratio of 1:3 (primary solvent:SDS/water) by vol.%. The mixture was then shaken until an emulsion was formed. Approximately 6 mL of this emulsion was transferred to the target cup, which was pre-cooled to − 196°C, ensuring rapid freezing of the emulsion to prevent flocculation.

Five solvents (toluene, pseudocumene, cyclopentantone, dichlorobenzene, trichlorobenzene) were used as the primary solvents in emulsion targets (all relevant solvent qualities shown in Table I). In order for a primary solvent to be an ideal candidate for RIR-MAPLE, it must have a low vapor pressure to prevent sublimation of the frozen target while under vacuum in the growth chamber. The primary solvent also must have low solubility in water to maintain emulsion stability. In most cases, the selected primary solvent dissolves the polymer effectively, but in the case of PFO, poor solvents were included because they are used to increase the concentration of β-PFO in spin-coated films.

The final emulsion was flash frozen in the target cup after vigorous shaking. The deposition time varied from 1 h to 4 h with a typical film thickness of approximately 50 nm. The Er:YAG laser was pulsed at 2 Hz with a laser fluence in the range of 1.6–1.8 J/cm^2. During deposition, the target cup rotated at a rate of 4 rotations/min for uniform ablation, the substrate rotated at a rate of 11 rotations/min, and the target-to-substrate distance was 7 cm. The chamber vacuum was maintained by a turbomolecular pump, allowing for excess solvent to be pumped away throughout the deposition. Films were deposited on 1 × 1 cm^2 silicon and glass substrates for use in materials characterization. The substrate growth temperature was investigated also, with temperatures ranging from 10°C (no temperature control) to 100°C.

It is important to note that the emulsions used in this process are complex, comprising five different components, and theories do not exist to describe the emulsified polymer particle sizes. In fact, the interaction of these different components can yield extremely unpredictable results. Therefore, different aspects of the emulsion preparation and deposition are explored to determine the impact on the emulsified particle size, surface morphology, and optical characteristics (i.e., presence of β-PFO). While some emulsion conditions yield very poor films, the results enable improvements to be made to the emulsion preparation such that the films become smoother, pinhole-free, and contain more of the semi-crystalline phase domain. It is also important to note that the most relevant factor regarding surface roughness is the surface roughness compared to the overall film thickness. If the roughness is comparable to the film thickness, in general the film quality is poor. This interdependence of surface roughness and film thickness is described by a normalized quality factor (defined as surface roughness divided by film thickness). The quality factor is included for all deposited films (Tables I, II, III, IV, and V). From experience, a reasonable quality factor for the fabrication of devices is ∼ 0.3 or less.

Materials Characterization

Ultraviolet–visible absorbance (UV–Vis) and photoluminescence (PL) spectroscopy measurements are sufficient to identify the crystallinity of PFO films.[29] In addition to the dominant characteristic peak at 380 nm caused by an increase in conjugation length, UV–Vis absorbance shows a

characteristic shoulder at 430 nm when β-PFO is present in the film. In the presence of β-PFO, the characteristic PL peak at 428 nm for α-PFO demonstrates a red-shift to 442 nm.[30] Emission from this red-shifted peak is far greater than the 428 nm peak, even for low concentrations of β-PFO. The UV–Vis absorbance spectra of thin films deposited by RIR-MAPLE were measured using the Shimadzu UV-3600 UV–Vis-NIR Spectrophotometer to compare the amount of ß-PFO present by the relative intensities of the amorphous (α-PFO) and crystalline (β-PFO) peaks. PL spectroscopy was performed using Horiba Jobin–Yvon LabRam ARAMIS, with photo-excitation from a 325 nm HeCd laser.

Atomic force microscopy (AFM) measurements of root mean squared (RMS) surface roughness and film thickness were conducted to determine the surface quality of each film using a Digital Instruments Dimension 3100 in tapping mode. A quality factor was defined as the RMS surface roughness divided by the film thickness, such that a smaller value indicates smoother films (< 0.2 was deemed sufficient for low contact resistance in devices). A FEI XL30 Scanning Electron Microscope was used to take detailed images of the films to analyze the effect of polymer concentration on film morphology. Magnification was set to 10,000X and the accelerating voltage was 5 kV. DLS was performed using the Nano Plus HD Particle Sizer, which implements an auto-correlation function to relate particle motion to particle diameter through the concept of Brownian motion and the Stokes–Einstein relationship. Measurements were made in the emulsion phase using glass cuvettes at 25°C with the accumulation time set to 5 s to avoid measuring a settled emulsion.

RESULTS AND DISCUSSION

Five different primary solvents were investigated in PFO emulsion target recipes for thin film deposition by RIR-MAPLE. The polymer concentration used in the emulsions was 5 mg/mL, the target emulsion recipe was 1:0.25:3 (primary solvent:phenol:water) by %vol, and the deposition time was set to 4 h. Table I shows the primary solvent properties and resulting thin film surface morphology after deposition by RIR-MAPLE, while Fig. 1 shows the corresponding AFM images and the photoluminescence and UV–Vis absorbance spectra. Cyclopentanone yielded the roughest film with large polymer aggregates, while trichlorobenzene yielded the smoothest film. Importantly, as demonstrated by PL and UV–Vis absorbance spectra, the presence of β-PFO was observed only for dichlorobenzene and trichlorobenzene primary solvents. The fact that no β-PFO was observed in thin films deposited from cyclopentanone is interesting because this solvent does yield β-PFO in solution-based deposition.[8,10] However, cyclopentanone does not possess important properties required for the primary solvent in RIR-MAPLE target emulsions (i.e., low vapor pressure and low solubility-in-water), therefore the deposited films had low film quality. Due to lower RMS surface roughness and higher β-PFO content in films deposited using tricholorobezene as the primary solvent, this solvent was selected for all subsequent RIR-MAPLE deposition studies in this

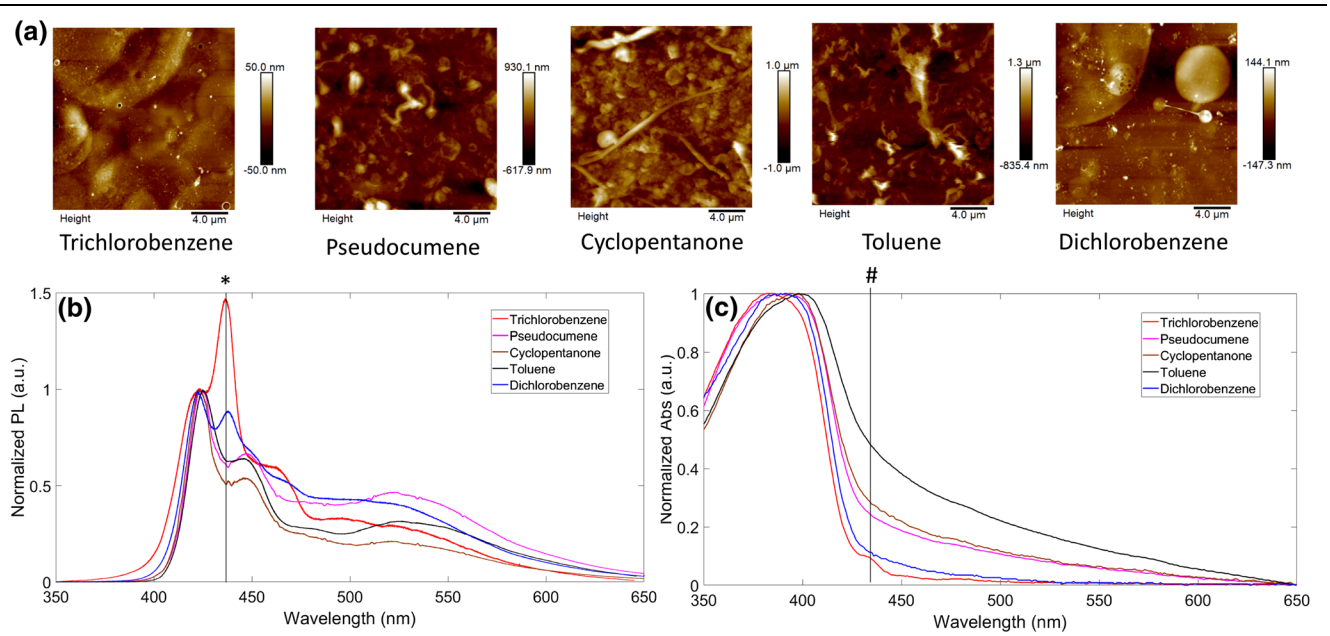

Fig. 1. AFM images (20 μm $\times$ 20 μm with different scales for the image height) (a), PL spectra (b), and UV–Vis absorbance spectra (c) of films deposited by emulsion-based, RIR-MAPLE using different primary solvents in the emulsion target. The red-shifted β-PFO luminescence peak is indicated by (*), and the β-PFO absorbance peak is indicated by (#).

Table II. Film surface morphology and emulsion particle sizes for PFO films deposited by emulsion-based, RIR-MAPLE with different emulsion mixing times (the indicated error represents the standard deviation for each measurement determined from three AFM images in different locations across the film)

Emulsion mixing time	Thickness (nm)	Roughness (nm)	Quality factor	Particle size (nm)
0 min	19.5 ± 3.9	18.2 ± 1.2	0.93	1680
5 min	6.8 ± 3.1	17.3 ± 4.3	2.5	40000
10 min	25.4 ± 9.2	13.9 ± 0.9	0.55	75000
15 min	22.7 ± 6.5	19.2 ± 6.8	0.85	100000
20 min	53.7 ± 6.6	26.8 ± 5.6	0.5	100000

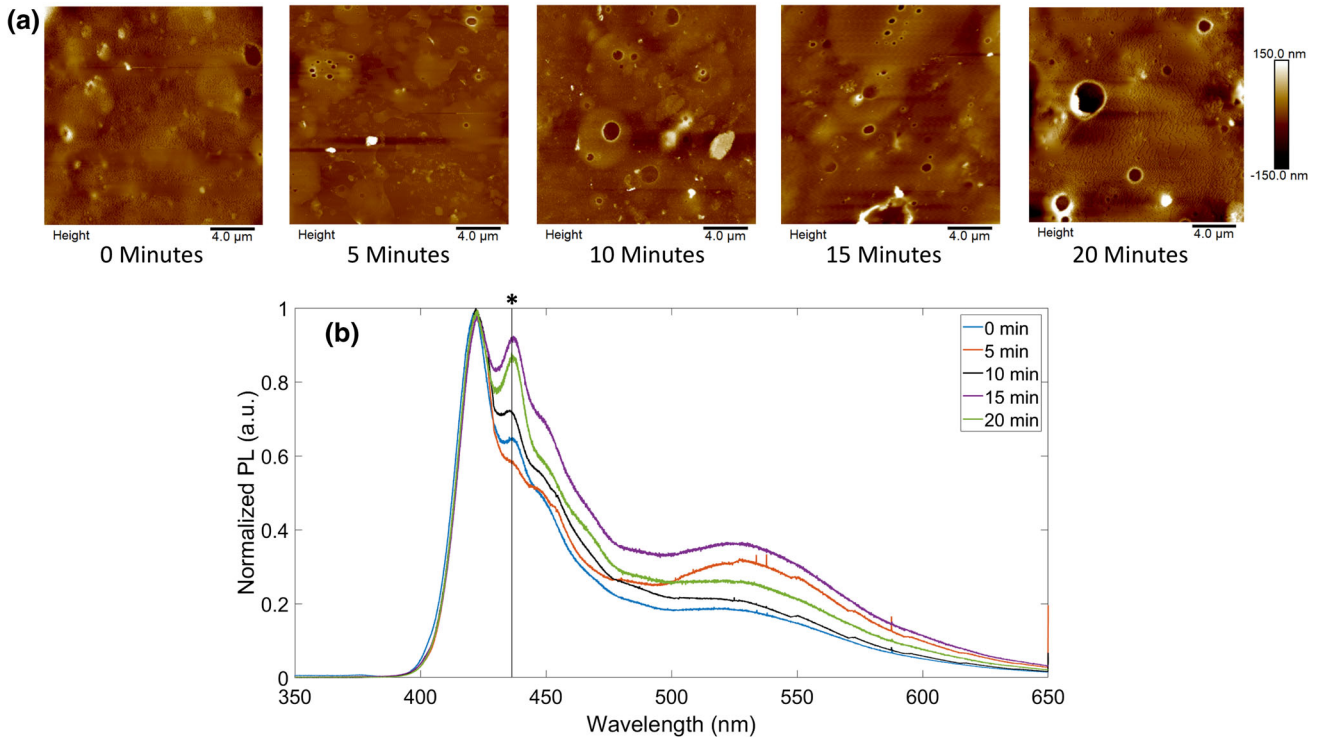

Fig. 2. AFM images (20 μm × 20 μm) (a) and PL spectra (b) of films deposited by emulsion-based, RIR-MAPLE using different emulsion mixing times. The red-shifted β-PFO luminescence peak is indicated by (*).

work. It is also important to note that the trichlorobenzene primary solvent did result in the observation of some minor pinholes in the film that could be problematic for devices.

Previous work to promote β-PFO has shown, conclusively, that crystalline domains form through self-interactions of the side chains.[31] Therefore, to increase the concentration of β-PFO, the length of time for which the RIR-MAPLE emulsion target was mixed prior to freezing was increased. Higher polymer concentration has also been shown to increase self-interactions, so a polymer concentration of 20 mg/mL was used for the emulsion target preparation. As a result of the higher polymer concentration, the deposition time was reduced to 1 h to compensate for more rapid deposition. Five mixing conditions were studied using the standard emulsion ratio from the primary solvent study (1:0.25:3 of primary solvent:phenol:water by %vol.). The emulsions were mixed for 0, 5, 10, 15, and 20 min at 800 RPM on a hotplate set to 35°C. Each emulsion was measured with DLS to determine the emulsified polymer particle size, and deposited films were characterized by AFM and PL. Table II shows the thin film surface morphology after deposition by RIR-MAPLE and the emulsified particle size, while Fig. 2 shows the corresponding AFM images and PL spectra. In general, the film surface morphology did not change significantly as the emulsion mixing time increased. In contrast, the emulsified particle size increased as the emulsion mixing time increased. In addition, the content of β-PFO in the deposited films increased as the mixing time increased, with the highest content occurring for mixing times of 15 or 20 min. Unfortunately, the presence of pinholes also increased as the emulsion mixing time increased.

Table III. Film surface morphology and emulsion particle sizes for PFO films deposited by emulsion-based, RIR-MAPLE with different phenol concentrations (1:*x*:3, primary solvent: secondary solvent: water) (the indicated error represents the standard deviation for each measurement determined from three AFM images in different locations across the film)

Secondary solvent phenol concentration (*x*)	Thickness (nm)	Roughness (nm)	Quality factor	Particle size (nm)
0	N/A	6.6 ± 1.4	N/A	0
0.15	31.4 ± 13	24.4 ± 8.6	0.78	10000
0.25	53.7 ± 6.6	26.8 ± 5.6	0.5	100000
0.35	38.8 ± 9.4	28.3 ± 17	0.73	40000
0.5	31 ± 1.3	21.6 ± 13	0.7	2000

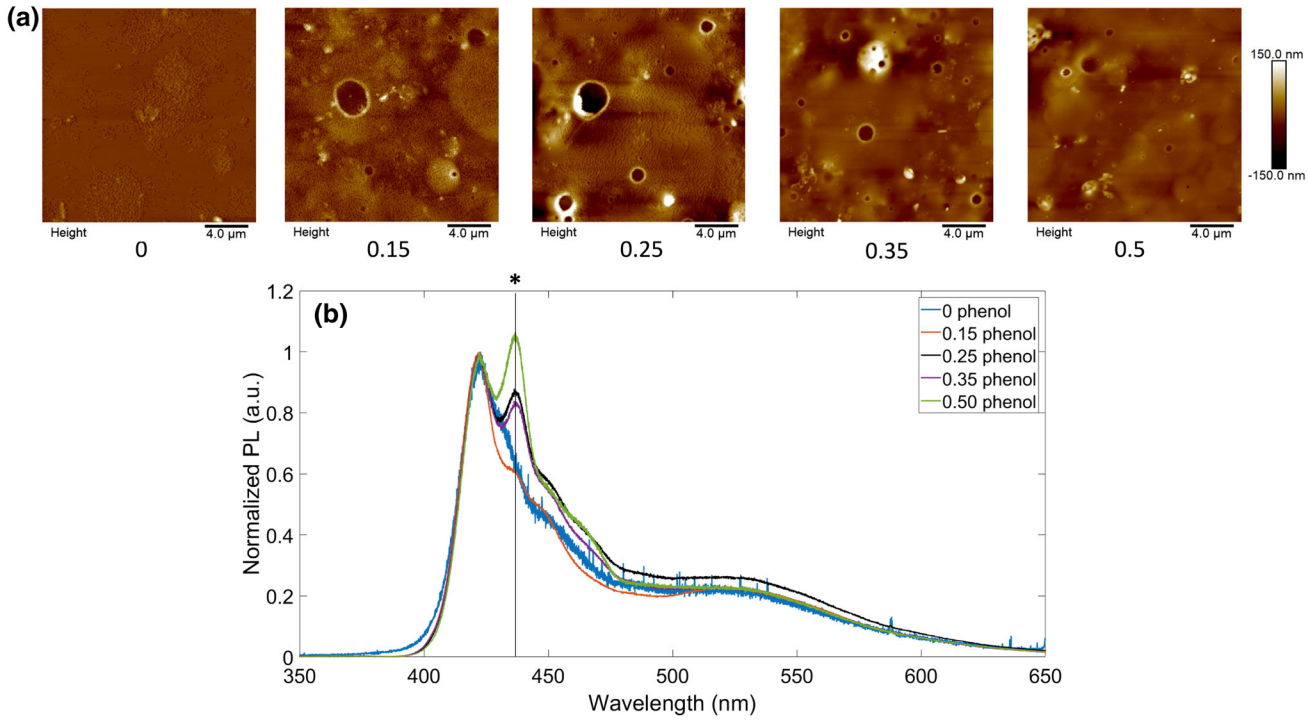

Fig. 3. AFM images (20 μm × 20 μm) (a) and PL spectra (b) of films deposited by emulsion-based, RIR-MAPLE with different concentrations of the secondary solvent, phenol. The red-shifted β-PFO luminescence peak is indicated by (*).

Because the use of secondary solvents, or additives, has been shown to promote β-PFO,[17,32] the concentration of phenol within the target emulsion was investigated to determine if the content of crystalline domains in PFO could be increased. Using trichlorobenzene as the primary solvent and a polymer concentration of 20 mg/mL, five emulsions were prepared and allowed to mix on a hotplate at 35°C for 20 min, each containing a different ratio of the secondary solvent phenol. The target emulsion ratio used was primary solvent:secondary solvent:water (by vol.%) of 1:*x*:3, where *x* represents the ratio of the phenol. This phenol concentration was varied such that x = 0, 0.15, 0.25, 0.35, 0.5. Each emulsion was measured with DLS to determine the emulsified polymer particle size, and deposited films were characterized by AFM and PL.

Table III shows the thin film surface morphology after deposition by RIR-MAPLE and the emulsified particle size, while Fig. 3 shows the corresponding AFM images and PL spectra. The film surface properties were comparable for all films, and the emulsified particle size seemed to peak around a phenol concentration of 0.25. AFM images demonstrated pinholes in all films with the phenol secondary solvent; however, without phenol, a contiguous polymer film was not deposited. Increasing the phenol concentration within the target emulsion yielded a larger concentration of β-PFO, as demonstrated by the PL spectra, which could indicate that phenol concentration beyond its solubility-in-water (0.078 vol.% @ 20°C) caused the secondary solvent to interact more strongly with the polymer.[33]

Table IV. Film surface morphology for PFO films deposited by emulsion-based, RIR-MAPLE with various heating conditions for the substrate through deposition (the indicated error represents the standard deviation for each measurement determined from three AFM images in different locations across the film)

Condition	Thickness (nm)	Roughness (nm)	Quality factor
Passive (uncontrolled)	53.7 ± 6.6	26.8 ± 5.6	0.5
25° C	40.8 ± 10.4	17.3 ± 6.3	0.42
50° C	75.5 ± 10.9	18.7 ± 2.9	0.25
100° C	35.0 ± 8.7	20.5 ± 4.2	0.59

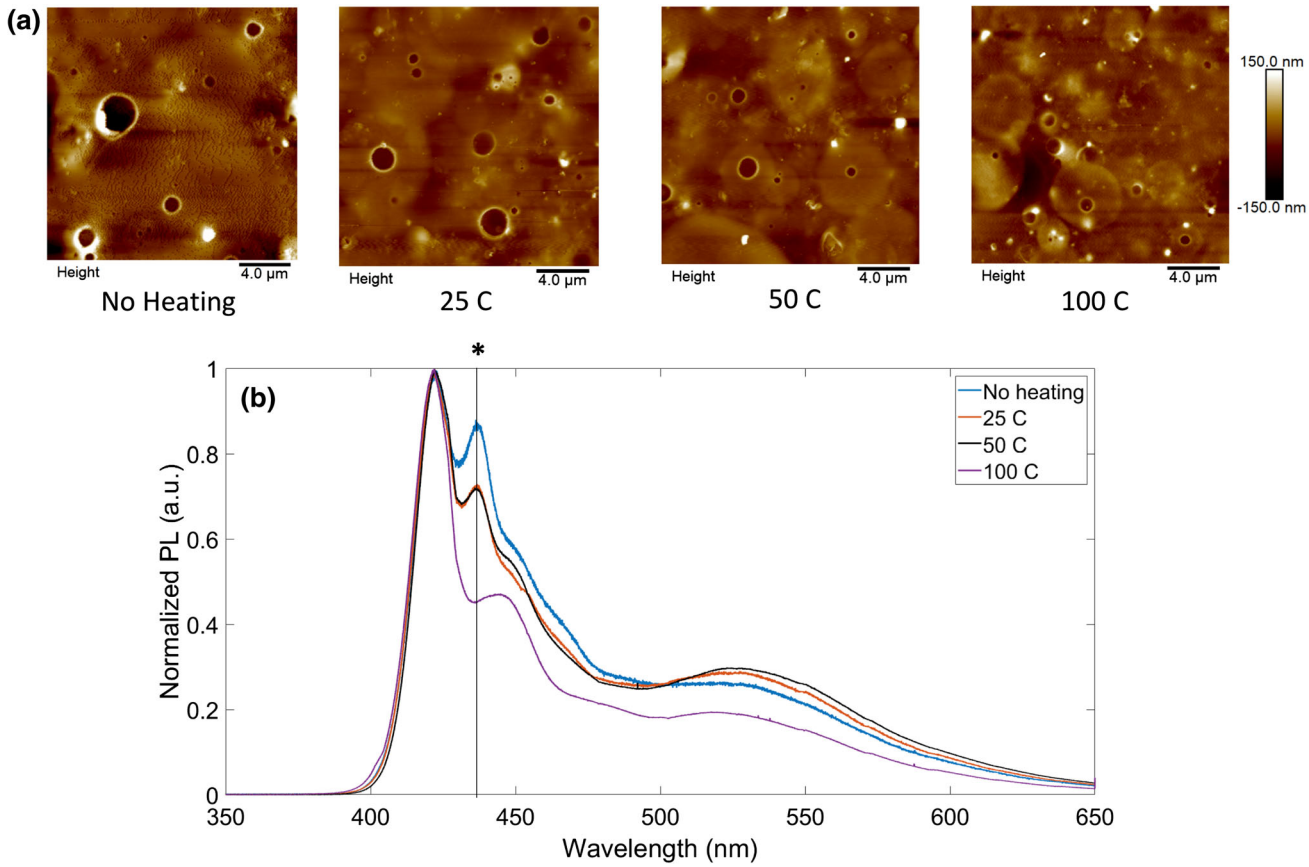

Fig. 4. AFM images (20 μm × 20 μm) (a) and PL spectra (b) of films deposited by emulsion-based, RIR-MAPLE with different substrate growth temperatures. The red-shifted β-PFO is indicated by (*).

For each of the previous studies, the observation of pinholes in the deposited films became more frequent with higher concentration of β-PFO. The likely cause of these pinholes is the slow evaporation of any primary solvent that reached the substrate, coupled with the fast deposition rate of PFO due to the high polymer concentration (20 mg/mL). The RIR-MAPLE system is equipped with a substrate heater managed by a Eurotherm system, allowing for precise control over the temperature of the substrate. Therefore, the substrate growth temperature was varied to determine if the additional thermal energy could help eliminate the observed pinholes: passive (or no substrate heating, ~ 10°C), 25°C, 50°C, and 100°C growth temperatures were investigated. Figure 4 shows the corresponding AFM images and PL spectra. The width and depth of the observed pinholes decreased as the substrate growth temperature increased due to more rapid evaporation of the trichlorobenzene primary solvent that reached the substrate via entanglement with the polymer. Table IV shows that a substrate growth temperature of 50°C yielded the lowest quality factor, indicating the smoothest film. However, the elevated substrate growth temperatures also decreased the concentration of β-PFO in the films. β-PFO was completely removed from the film for a substrate growth temperature of 100°C.

Finally, the DLS particle size measurements reported for this study, deposited from 20 mg/mL

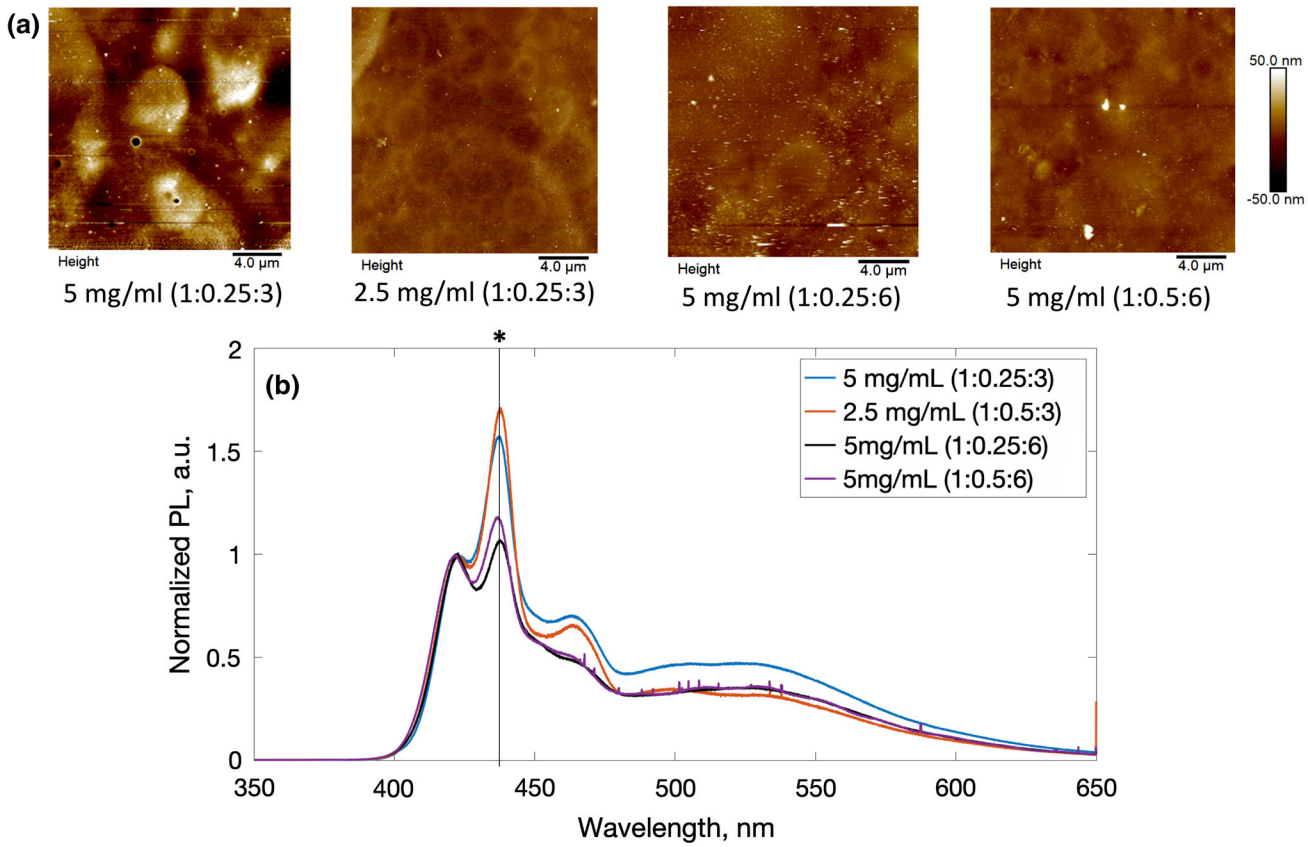

Fig. 5. AFM images (20 μm $\times$ 20 μm) (a), PL spectra (b) of films deposited by emulsion-based, RIR-MAPLE using different emulsion ratios of the primary solvent, secondary solvent, and water matrix. The red-shifted β-PFO is indicated by (*), and the β-PFO absorbance peak is indicated by (#).

PFO concentration in emulsion recipes of 1:0.25:3 for the primary solvent:secondary solvent:water, indicated that the PFO target emulsions have very large emulsified particle sizes, which are not likely to be spherical. This hypothesis is supported by the presence of pinholes in the deposited films that indicate the primary solvent is becoming trapped or entangled within complex polymer structures inside the emulsion. In order to promote spherical particles that yield smooth films with high quality,[21] the polymer concentration was lowered from 20 mg/mL to either 5 mg/mL or 2.5 mg/mL. This reduction in polymer concentration also decreases the deposition rate, so the deposition time was increased to 4 h to achieve the desired film thickness. The substrate growth temperature was set to 50°C to try to balance the trade-off between β-PFO content and the presence of pinholes. In order to further explore the hypothesis that pinholes result from solvent entanglement with large, non-spherical emulsified particles, the overall water ratio in the emulsion recipe was increased to 1:x:6 to slow the deposition rate by further diluting the overall polymer concentration, thereby enabling the primary solvent, trichlorbenzene, to evaporate from the substrate or film surface prior to deposition of additional material. The phenol ratio in this high-water content emulsion, x, was increased from 0.25 to 0.5 to ensure that the phenol concentration remained at the solubility limit in water for stable emulsions. Figure 5a shows the measured AFM images. The left-most image in Fig. 5a for the 5 mg/mL, 1:0.25:3 emulsion recipe shows pinholes in the film due to trapped solvent, consistent with the fact that it was deposited at a rate approximately four times faster than the remaining three films. AFM images shown in Fig. 5a also indicate that maintaining the phenol concentration at its solubility level in water (x:0.25:3), in terms of the emulsion recipe ratio) resulted in films free of undissolved polymer, in contrast to the 5 mg/mL, 1:0.25:6 growth condition. In Fig. 6, SEM images of two films (a) 20 mg/mL, 1:0.25:3 and (b) 5 mg/mL, 1:0.5:6 are shown, demonstrating the expected reduction in the surface density of pinholes.

Table V shows the thin film surface morphology after deposition by RIR-MAPLE with different polymer concentrations and emulsion ratios, as well as the emulsified particle sizes. The most obvious trend is that the particle size decreased by two orders of magnitude for the high-water content emulsions. Most likely, this reduction in particle

Table V. Film surface morphology and emulsion particle sizes for PFO films deposited by emulsion-based, RIR-MAPLE with various polymer concentrations and emulsion ratios (the indicated error represents the standard deviation for each measurement determined from three AFM images in different locations across the film)

Condition	Thickness (nm)	Roughness (nm)	Quality factor	Particle size (nm)
5 mg/mL 1:0.25:3	110.1 ± 13.5	16 ± 0.57	0.15	10,000
2.5 mg/mL 1:0.25:3	26.8 ± 3.9	13.6 ± 4.6	0.51	40,000
5 mg/mL 1:0.25:6	16.1 ± 1.6	8.0 ± 0.93	0.50	600
5 mg/mL 1:0.5:6	26.6 ± 1.9	9.6 ± 3.3	0.36	500

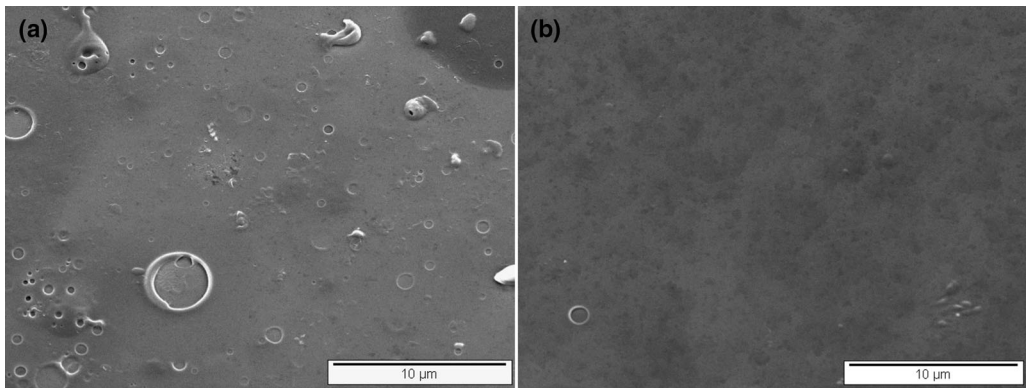

Fig. 6. SEM images of PFO thin films deposited by emulsion-based RIR-MAPLE using 20 mg/mL polymer concentration in an emulsion ratio for primary solvent:secondary solvent:water of 1:0.25:3 (a) and using 5 mg/mL polymer concentration in an emulsion ratio of 1:0.5:6 for primary solvent:secondary solvent:water (b).

size is related to the overall surfactant concentration in the emulsions. The surfactant concentration in water was held constant at 0.001 wt.% for the low- and high-water content emulsions; however, the total amount of surfactant in the emulsion, with respect to the polymer concentration, increased for the high-water content emulsion such that there was greater likelihood of forming smaller, spherical particles. However, Fig. 5b indicates that the emulsion recipes of 5 mg/mL, 1:0.25:3 and 2.5 mg/mL, 1:0.25:3, both low-water content emulsions, contain the most β-PFO. Therefore, larger particles sizes with more entangled solvent enable the semi-crystalline β-PFO to form during film deposition, as demonstrated in a previous study using slowly evaporating solvents to form β-PFO crystals.[34]

Figure 7 shows UV–Vis absorbance spectra of a film deposited from the emulsion condition with the largest β-PFO concentration (2.5 mg/mL 1:0.25:3) and pristine PFO dissolved in TCB in a cuvette. The α-PFO and β-PFO absorbance peaks are labelled. While the relative intensity and linewidth of each spectrum changes due to the impact of changing β-PFO concentration by RIR-MAPLE deposition, the peak position remains the same, confirming that the optical signatures can be used to characterize the presence of β-PFO in the film.

CONCLUSIONS

Through the use of emulsion-based RIR-MAPLE, numerous films were deposited in order to explore the impact of emulsion conditions on the emulsified polymer particle size, film surface morphology, and β-PFO content, with the overall goal of identifying an emulsion condition in which β-PFO semi-crystalline phase domains can be deposited without the introduction of pinholes. Ultimately, β-PFO content was increased in a pinhole-free film by: (1) using trichlorobenzene as the primary solvent, which is a poor solvent of PFO and enables the semi-crystalline phase domains to form; (2) using a PFO concentration *in water* of approximately 0.83 mg/ml (i.e., 5 mg/ml of PFO in TCB in 6 ml of water or 2.5 mg/ml of PFO in TCB in 3 mL of water), which reduces the deposition rate and permits the primary solvent within the particle to evaporate in vacuum during deposition such that the primary solvent is not trapped within the film and cannot lead to subsequent pinholes; (3) setting the concentration of

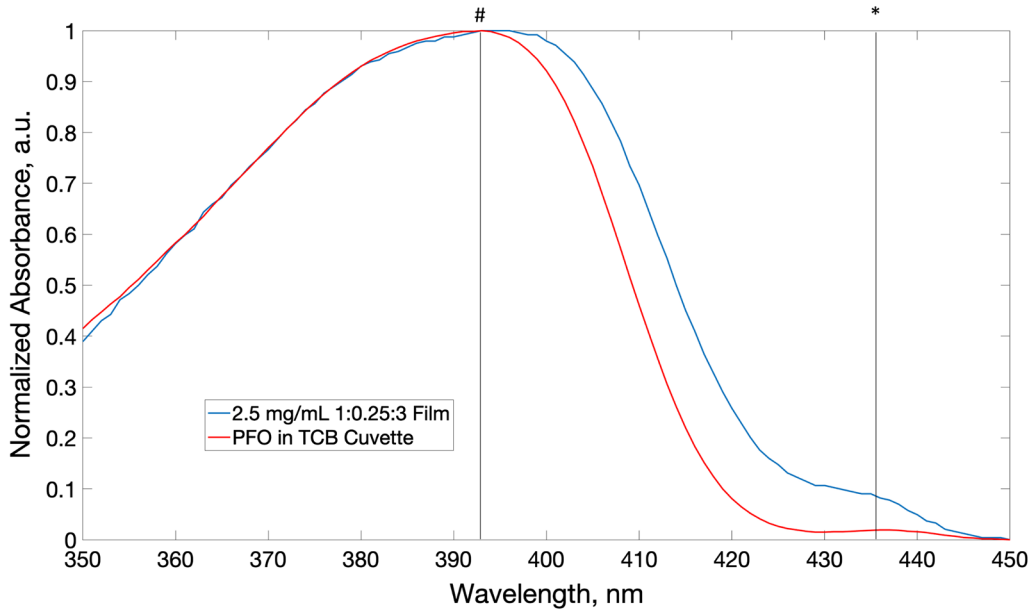

Fig. 7. UV-Vis absorbance spectra of PFO dissolved in trichlorobenzene in a cuvette and a PFO film deposited via emulsion-based, RIR-MAPLE using 2.5 mg/mL polymer concentration and emulsion ratio of 1:0.25:3 (primary solvent:secondary solvent:water). The α-PFO peak and β-PFO shoulder are indicated on the spectra for reference.

phenol in water to $\sim$ 0.083 g/mL, which is the solubility-in-water of phenol (corresponding to an emulsion recipe of x:0.25:3 primary solvent:phenol:water) and using an emulsion mixing time of 20 min, both of which stabilize the emulsion; and (4) depositing the film at a substrate temperature of 50°C, which eliminates pinholes while still allowing the formation of β-PFO. Following these emulsion design principles, two recipes, namely 2.5 mg/mL, 1:0.25:3 and 5 mg/mL, 1:0.5:6, were used to deposit pinhole-free films containing approximately 6% of the β-PFO semi-crystalline phase domain.

The deposition of pinhole-free thin films containing β-PFO by emulsion-based, RIR-MAPLE is an important result because it could enable a direct investigation of the impact of this crystalline phase on the performance of PFO-based LEDs. Such studies have been difficult to accomplish using spin-casting because of the degradation in surface quality (i.e., presence of pinholes) that occurs when poor solvents or additives are used to promote β-PFO.[17,20] In addition, in solution-based deposition of these films, as the β-PFO content increases, the film quality decreases. In contrast, this study has demonstrated that the films remain pinhole free as the content of β-PFO increases, as indicated in the AFM images and PL spectra of Fig. 5 for the two emulsion recipes mentioned above. Therefore, future work will focus on emulsion-based RIR-MAPLE growth of PFO thin films to increase the content of β-PFO to at least 42% in order to maintain stability.[20] In addition, device performance of PFO-based LEDs with varying concentrations of the crystalline phase will be measured to determine the impact on device performance, especially the turn-on voltage, which could help lead to longer lifetimes of blue LEDs if significantly reduced.

ACKNOWLEDGMENTS

This material is based upon work supported by the National Science Foundation under Grant No. NSF CMMI-1727572.

REFERENCES

1. Y. Zhao, Y. Zhou, Y. Yang, J. Xu, Z.D. Chen, and Y. Jiang, *Mater. Lett.* 219, 201 (2018).
2. Y.J. Park, Y.S. Kang, and C. Park, *Eur. Polym. J.* 41, 1002 (2005).
3. D.M. de Leeuw, M.-J. Spijkman, P.W.M. Blom, M. Li, I. Katsouras, H.J. Wondergem, and K. Asadi, *Nat. Mater.* 12, 433 (2013).
4. A. Salimi and A.A. Yousefi, *J. Polym. Sci. Part B Polym. Phys.* 42, 3487 (2004).
5. A.J. Cadby, P.A. Lane, H. Mellor, S.J. Martin, M. Grell, C. Giebeler, D.D.C. Bradley, M. Wohlgenannt, C. An, and Z.V. Vardeny, *Phys. Rev. B Condens. Matter Mater. Phys.* 62, 15604 (2000).
6. M. Knaapila and A.P. Monkman, *Adv. Mater.* 25, 1090 (2013).
7. Y. Chen, X. You, X. Zhang, X. Zhang, B. Liu, W. Lai, and W. Huang, *J. Appl. Polym. Sci.* 134, 6 (2017).
8. A.L.T. Khan, P. Sreearunothai, L.M. Herz, M.J. Banach, and A. Köhler, *Phys. Rev. B Condens. Matter Mater. Phys.* 69, 085201 (2004).
9. P. Prins, F.C. Grozema, B.S. Nehls, T. Farrell, U. Scherf, and L.D.A. Siebbeles, *Phys. Rev. B Condens. Matter Mater. Phys.* 74, 10 (2006).
10. A. Hayer, A.L.T. Khan, R.H. Friend, and A. Köhler, *Phys. Rev. B Condens. Matter Mater. Phys.* 71, 1 (2005).
11. X. Zhang, Q. Hu, J. Lin, Z. Lei, X. Guo, L. Xie, W. Lai, and W. Huang, *Appl. Phys. Lett.* 103, 153301 (2013).
12. C.W. Cone, R.R. Cheng, D.E. Makarov, and D.A. Vanden Bout, *J. Phys. Chem. B* 115, 12380 (2011).
13. H.H. Lu, C.Y. Liu, C.H. Chang, and S.A. Chen, *Adv. Mater.* 19, 2574 (2007).

14. J. Shinar and R. Shinar, *J. Phys. D Appl. Phys.* 41, 133001 (2008).
15. R.H. Friend, R.W. Gymer, A.B. Holmes, J.H. Burroughes, R.N. Marks, C. Taliani, D.D.C. Bradley, D.A. Dos Santos, J.L. Bredas, M. Logdlund, and W.R. Salaneck, *Nature* 397, 121 (1999).
16. H. Wan, S. Bai, H. Li, J. Ding, B. Yao, Z. Xie, L. Wang, and J. Zhang, *J. Lumin.* 131, 1393 (2011).
17. J. Peet, E. Brocker, Y. Xu, and G.C. Bazan, *Adv. Mater.* 20, 1882 (2008).
18. N. Gupta, R. Grover, D.S. Mehta, and K. Saxena, *Org. Electron. Phys. Mater. Appl.* 34, 276 (2016).
19. Y. Fang, E. Gu, L. Chi, R. Xia, W. Huang, Q. Zhang, G. Hai, and X. Li, *Molecules* 22, 315 (2017).
20. B. Liu, T. Li, H. Zhang, T. Ma, J. Ren, B. Liu, B. Liu, J. Lin, M. Yu, L. Xie, and D. Lu, *J. Phys. Chem. C* 122, 14814 (2018).
21. W. Ge, N.K. Li, R.D. McCormick, E. Lichtenberg, Y.G. Yingling, and A.D. Stiff-Roberts, *ACS Appl. Mater. Interfaces* 8, 19494 (2016).
22. R.D. McCormick, E.D. Cline, A.S. Chadha, W. Zhou, and A.D. Stiff-Roberts, *Macromol. Chem. Phys.* 214, 2643 (2013).
23. R.D. McCormick, J. Lenhardt, and A.D. Stiff-Roberts, *Polymers (Basel).* 4, 341 (2012).
24. R. Pate, K.R. Lantz, and A.D. Stiff-Roberts, *IEEE J. Sel. Top. Quantum Electron.* 14, 1022 (2008).
25. T. Tunno, A.P. Caricato, M.E. Caruso, A. Luches, M. Martino, F. Romano, D. Valerini, and M. Anni, *Appl. Surf. Sci.* 253, 6461 (2007).
26. F. Mariano, A.P. Caricato, G. Accorsi, C. Leo, M. Cesaria, S. Carallo, A. Genco, D. Simeone, T. Tunno, M. Martino, G. Gigli, and M. Mazzeo, *J. Mater. Chem. C* 4, 7667 (2016).
27. W. Zhao, T. Cao, and J.M. White, *Adv. Funct. Mater.* 14, 783 (2004).
28. K.A. Luck, H.N. Arnold, T.A. Shastry, T.J. Marks, and M.C. Hersam, *J. Phys. Chem. Lett.* 7, 4223 (2016).
29. S.H. Chen, A.C. Su, and S.A. Chen, *J. Phys. Chem. B* 109, 10067 (2005).
30. M. Grell, D.D.C. Bradley, G. Ungar, J. Hill, and K.S. Whitehead, *Macromolecules* 32, 5810 (1999).
31. D.W. Bright, F.B. Dias, F. Galbrecht, U. Scherf, and A.P. Monkman, *Adv. Funct. Mater.* 19, 67 (2009).
32. L. Huang, X. Huang, G. Sun, C. Gu, D. Lu, and Y. Ma, *J. Phys. Chem. C* 116, 7993 (2012).
33. D. Lu, T. Ma, Z. Bai, H. Zhang, J. Ren, T. Li, B. Liu, and X. Li, *Polymer (Guildf)* 103, 299 (2016).
34. L. Xu, J. Zhang, J. Peng, and F. Qiu, *J. Polym. Sci., Part B Polym. Phys.* 53, 633 (2015).